Porous Media Flow Transitioning into the Forchheimer Regime: a PIV Study

J. K. Arthur

Department of Mechanical and Manufacturing Engineering, Schulich School of Engineering, University of Calgary, 2500 University Drive, Calgary, Alberta, T2N 1N4, Canada

†*Corresponding Author Email: james.arthur@ucalgary.ca*

ABSTRACT

One of the essential areas of the study of transport in porous medium is the flow phenomena at the onset of inertia. While this area has attracted considerable research interest, many fundamental questions remain. Such questions relate to things such as the nature of the multi-dimensional velocities of the flow, the evolution of inertia, the differences in flow phenomena at various complexity of porous media, and the best constitutive equation for the flow. To resolve some of these questions, the present research program was designed to experimentally investigate pressure-driven flow through two- and three-dimensional porous media at the onset of inertia. Specifically, the goals in view were to obtain velocity data and pressure measurements, apply the benchmark experimental data to study the evolution of inertia, distinguish differences in such evolution with respect to the parameters of the porous media, and to establish the constitutive equation that best describes the porous media flow when inertia sets in. What particularly sets this work apart, is the use of particle image velocimetry (PIV) – an experimental technique that captures multi-dimensional flow quantities, as opposed to mere flow rates. Using PIV then, detailed velocity measurements were conducted for flows through model porous media of solid volume fraction 6%, 12%, and 22%. The velocities were spatially averaged to obtain average streamwise and transverse components. In addition to the velocity measurements, differential pressure measurements were obtained using pressure-measurement gauges and transducers. The pressure and velocity data sets were then statistically analyzed and presented to provide a complete set of experimental data to characterize the flow through the model porous media. The results show that the velocity flow domain is dictated by the streamwise velocities, which are at least an order of magnitude greater than the transverse components. Furthermore, pressure drag was found to increase with compactness and complexity of the porous media. While inertia increases exponentially from particle Reynolds number ~ 1 – 3 onwards, it is apparently subdued by the form drag that tends to dominate the flow through complex media. Overall, the flow at the onset of inertia is best described by a power law. These results provide insights that are applicable to flows such as those near well bores and fractures where seepage velocities are relatively high.

Keywords: Particle image velocimetry; Porous media; Darcy; Forchheimer; Izbash; Inertia.

NOMENCLATURE

A	plane area	R^2	coefficient of reduction
a	Forchheimer equation parameter	U_d	streamwise seepage velocity
b	Forchheimer equation parameter	$U_{d,max}$	maximum streamwise seepage velocity
c	empirical term	u	streamwise velocity
d	rod diameter	V_d	transverse seepage velocity
dP_f/dx	streamwise pressure difference gradient	v	transverse velocity
f_{Ud}	friction factor	x	streamwise direction
f_{Vd}	friction factor	y	transverse direction
g	empirical term	z	spanwise direction
h	empirical term		
i	hydraulic gradient	α	empirical parameter
K	hydraulic conduction coefficient	β	empirical parameter
k	Darcy permeability	ε	empirical parameter
Q	volumetric flow rate	ϕ	solid volume fraction
Re_d	particle Reynolds number	μ_f	dynamic viscosity of fluid

ν kinematic viscosity of fluid ρ_f density of fluid

1. INTRODUCTION

There are several engineering applications where flow through porous media is of important relevance. Some examples include permeable reactive barriers, groundwater hydrology, filtration technology and oil and gas exploration. Porous media flow phenomena are largely considered under laminar conditions where inertial effects are immaterial. Darcy (1856) observed that for a steady-state flow in a uniform porous medium under such non-inertial conditions, there is a linear relationship between the volumetric flow rate Q passing through a porous bed of plane area A, and the applied hydraulic gradient i. The relationship is dependent on an unknown hydraulic conduction coefficient K. The relation, known as the Darcy law, is stated as:

$$K = \frac{Q}{Ai} \tag{1}$$

In differential equation terms, this law may also be written as (Arthur, 2012)

$$-\frac{dP_f}{dx} = \frac{\mu_f U_d}{k} \tag{2}$$

where dP_f / dx, μ_f, U_d and k are respectively the constant gradient of the streamwise pressure difference, the dynamic viscosity of the fluid, seepage velocity and the Darcy permeability.

Although the Darcy law is generally accepted to govern porous media flow, it does not cover all the practical ranges of flow in porous media. This is particularly the case for areas of application such as those near well bores, fractures and tight screens of cryogenic propellant tanks, where seepage velocities are relatively high. The regime at which the flow deviates from the Darcy law is known as the Forchheimer regime. Although the onset of this deviation is generally attributed to a more prominent inertial force (e.g. Chauveteau, 1965), the actual origins of these inertial forces have been the object of many speculations (Hlushkou and Tallarek, 2006). While some researchers ascribe this inertial force to pore roughness (Minsky, 1951), others point out that this stems from such factors as the microscopic inertial force (Ma and Ruth, 1993), inertial core development (Dybbs and Edwards, 1984), interstitial pore space curvature (Hayes *et. al.* 1995), viscous boundary layer formation (Whitaker, 1996), and the singularity of patterns of streamlines that is sometimes associated with microscale non-periodicity of flow (Panfilov *et al.* 2003).

Regardless of these propositions, it is safe to state that as a matter of general observation, as seepage velocities increase in porous media flows, a gradual transition occurs, resulting in a flow in which the relationship between the seepage velocity and the driving pressure gradient is no longer linear. In this case, inertia is no longer negligible and has to be accounted for in the flow description. In order to correct for the non-linearities in the inertial Forchheimer flow regime, Forchheimer (1901) proposed an *ad hoc* equation of the following form for an isotropic porous medium

$$-\frac{dP_f}{dx} = a U_d + b U_d{}^2 \tag{3}$$

Here, a is the ratio of the dynamic viscosity to an equivalent Forchheimer permeability, and b is the product of the inertial coefficient and the fluid density.

Equation (3), also known as the Forchheimer equation, is perhaps the most widely used formulation for describing inertial effects in steady laminar flow through porous media. Its veracity has been corroborated both experimentally (Sedghi-Asl *et al.* 2015) and theoretically (Marušic-Paloka and Mikleic, 2000). However, the certainty of the Forchheimer equation is also not without doubts on a number of issues. The first is that its empirical verifications rest mainly on global measurements of flow rates and pressure differences across various porous media sample. This means that details (particularly of velocity) may not have been fully captured in those bulk measurements. Further to this, there have also been a number of experiments that have been at variance with the Forchheimer equation. These include the notable experiments of Forchheimer (1930) and Barree and Conway (2004, 2005). In fact, after re-examining earlier reported data of Darcy (1856), Hazen (1895) and Chauveteau (1965), Firdaous *et al.* (1997) concluded that the data followed a cubic law. To re-enforce these observations, Ruth and Ma (1992) and Ma and Ruth (1993) also showed the non-uniqueness of the equation that governs the steady nonlinear flow, pointing out that any number of polynomials could be used to describe the nonlinear behavior of the flow. This conclusion is in concurrence with Mei and Auriault (1991) who had earlier shown that at low, finite velocities a homogenization technique yields a cubic law, not a quadratic law.

These latter findings are not surprising, given that other equations have been suggested in the past to describe inertial steady laminar flows in porous media (Basak, 1977). Forchheimer (1901) himself suggested two other equations of the following forms, which are relatively less known

$$-\frac{dP_f}{dx} = a U_d + b U_d{}^g \tag{4}$$

$$-\frac{dP_f}{dx} = a U_d + b U_d{}^2 + c U_d{}^3 \tag{5}$$

where g and c are empirical terms. Izbash (1931) also proposed an empirical power law of the form

$$-\frac{dP_f}{dx} = \varepsilon U_d{}^h \qquad (6)$$

and h are empirical parameters, depending on the flow conditions. Although this power law rivals the Forchheimer equation (as it is the preferred choice in modeling drainage systems; Bordier and Zimmer, 2000), its physical soundness seems to be relatively less established. White (1935), after analyzing dry air flow through packed towers (Scheidegger, 1960), also gave a correlation belonging to the family of Eq. (5), but setting h equal to 1.8. There have been other less known empirical and semi-empirical power laws by Escande (1953), Wilkinson (1956) and Slepicka (1961) which are reviewed by Basak (1977), all demonstrating the non-uniqueness of the Forchheimer equation to describe the inertial flow. There are other formulations that may also be seen as extensions of the Forchheimer equation. These, such as those of Wooding (1957) have been passed over because they are mainly suited for unsteady flows.

In view of the foregoing, the present research program seeks to experimentally investigate pressure-driven flow through two- and three-dimensional porous media to study the onset of inertia in porous media flow. Specifically, the goals are to apply benchmark experimental data to study the evolution of inertia, to distinguish differences in such evolution with respect to the parameters of the porous media, and to establish the constitutive equation that best describes the porous media flow when inertia sets in. Apart from the goals in view, what particularly sets this work apart from others, is the use of particle image velocimetry (PIV) – an experimental technique that captures multi-dimensional flow quantities – as opposed to mere global quantities. Particle image velocimetry allows for the instantaneous whole flow-field measurement of pore-scale two- and three-dimensional velocities from which averages of flow quantities can be obtained. Using a high-resolution PIV technique then, detailed velocity measurements were conducted both within the porous medium. To capture the variations of velocities in all directions various planes were measured along various sections along the span of the test section. The velocities were averaged spatially. In addition to the velocity measurements, differential pressure measurements were obtained using pressure-measurement gauges and transducers. The refined pressure and velocity data sets were then statistically analyzed and presented to provide a complete set of experimental data to characterize the flow through the model porous media and to determine the requisite constitutive equations.

2. EXPERIMENTAL METHOD

In this section, the experimental method is described. This includes the test channel, porous media models, velocity and pressure measurement set-ups, as well as the general experimental rig. Subsequently, an account is given of how certain preliminary measurement concerns regarding uncertainty and measurement procedure were resolved. An outline of the test conditions is then presented.

2.1 Test Channel and Porous Media

The tests were conducted in a 25-mm thick transparent acrylic channel of refractive index (RI) 1.47. The length, span, and depth of the test channel were respectively 500 mm, 115 mm and 83 mm. The channel was so designed to conduct flow through a central entry hole at the upstream end, then through a 200-mm flow conditioning section, and subsequently through a 300-mm test section, before exiting through another central hole at the downstream end. It should be noted that each of the long faces of the channel at the test section was reserved for either velocity or pressure measurements. The side reserved for pressure measurement was arrayed with pressure tap holes of 3.18 mm diameter.

In this work, regular arrays of circular rods are used to model real porous media. This was done because of the relative simplicity and adaptability of such model media in controlled studies, and the practical utility of such model in simulating real cases such as banks of heat exchanger tubes. Two kinds of models were tested, as shown in Fig. 1. For the first kind (hereafter called horizontal models), the rods were aligned in one direction (*i.e.* spanwise direction), to simulate a two-dimensional porous medium. In the second model kind (henceforth called mesh models), the rods were alternately arrayed in a regular fashion in both spanwise and transverse directions to simulate a three-dimensional porous medium. As for the test channel, each of the porous media models was constructed from acrylic rods, two side plates, and one lower acrylic plate, all of RI, 1.47. For models of circular rod of diameter $d = 3.18$ mm, the rods were arranged to achieve solid volume fractions ϕ of 6%, 12%, 22% respectively. To do this, rods were spaced at a distance l determined from:

$$l = d/2 \; \sqrt{(\pi/\phi)} \qquad (7)$$

The range of solid volume fraction was so selected to cover the entire range of solid volume of fibrous and dense porous media practically suitable for the PIV technique.

2.2 PIV System

Velocity measurements were obtained using a planar particle image velocimetry (PIV) system, schematized in Fig. 2(a). The system used in the present tests was made up of a source of illumination, a camera system, a synchronization hub, and a computer system. A laser generator providing a Nd-YAG 120 mJ/pulse laser at 532 nm wavelength of light, was connected to a lens system to provide a thin (~1.5mm) laser sheet to illuminate the flow. A *Dantec Dynamic HiSense* 4M digital charge coupled device (CCD) camera of 2048-pixel

by 2048-pixel chip and pitch 7.4 μm, was fitted with a C–mount 58 mm – 62 mm diameter EX Sigma lens. With such a camera system, images of the flow were captured in synchrony with the laser and computer. The synchronization was achieved using the hub connection. A *Dantec Dynamic DynamicStudio* v.2.30 commercial software, installed on the hard-drive of a desktop computer, was used to operate the PIV system, and to process the data that was acquired.
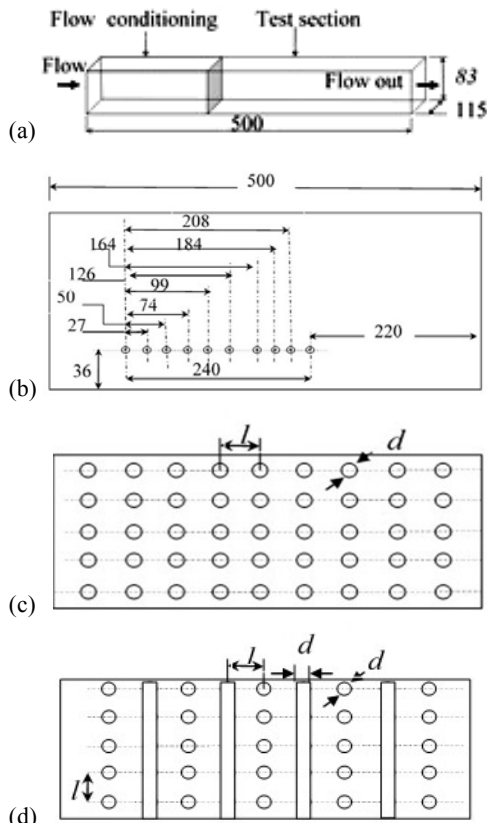

Fig. 1. Schematic of (a) test channel, (b) pressure measurement face of the channel, (c) front view of horizontal model porous medium, (d) front view of the mesh model porous medium. All numeric dimensions are in millimeters.

A *Cargille* Immersion liquid (Code 5040) of kinematic viscosity $\nu = 20 \times 10^{-6}$ m²/s (at 25°C), density $\rho_f = 848$ kg/m³ and RI = 1.47, was used as the working fluid. The fluid was in turn seeded with silver-coated hollow glass spheres of mean diameter 10 μm and specific gravity 1.4. With such properties, the particles were sufficiently large to scatter light that is detectable by the recording medium. Given that the particle settling velocity and response time (based on the working fluid and seeding particles) are approximately 1.77 μm/s and 7.98 ps, respectively, and therefore very small compared with the typical velocity and time scales used in the experiment, the particles were considered to follow the fluid faithfully.

2.3 Pressure Measurement System

Differential pressure measurements were consecutively made using two 4000 Series *Capsuhelic* pressure gauges, rated to measure pressures ranging from 0 to 0.5 and 0 to 1 inches of water respectively. These measurement devices were connected to the pressure ports on the test channel by a system of tubes, brass quick disconnect fixtures, and other accessory connectors (Fig. 2b). A DTD+ electronic transducer rated to measure 0 to 1 inches of water was also used. This transducer was connected to a digital Model Pax read-out meter and a personal computer to display the measurements.

2.4 Arrangement of Test Facility

The flow circuit of the test facility is schematized in Fig. 3. The facility consisted of the test channel with test models, a reservoir, a single speed centrifugal pump, two piston–spring loaded flow meters (to provide a quick readout of flow rate from the pump), interconnecting hoses, tubing, and valves. The test channel was seated in a set of metered acrylic plates so that the tank could be moved in the streamwise and lateral directions. The channel and the metered plates were both placed on a black PVC panel and supported on a structural frame at a 1-meter elevation off the ground. The laser and the camera were fixed on the frame mechanism in such a way that they could be traversed in a parallel plane. The camera and test channel were respectively fixed onto translation stages of a least count of 0.5 mm.
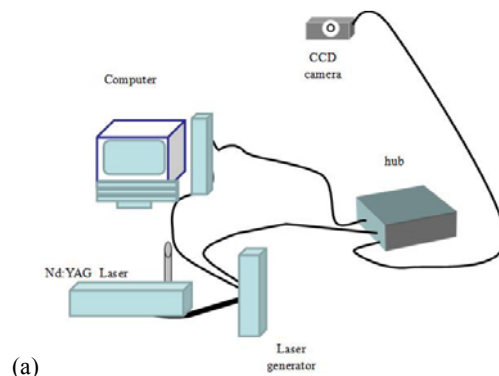

Fig. 2. (a) Schematic drawing of particle image velocimetry set-up; (b) A picture showing the rear end of the test channel fitted with pressure port connectors.
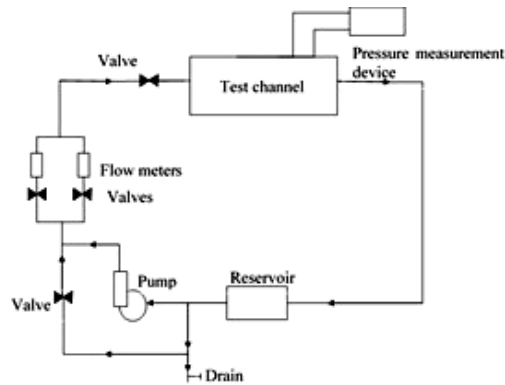
Fig. 3. Schematic diagram of the flow circuit.

2.5 Measurement Procedure

The seeded working fluid was recirculated through a flow circuit, starting from the reservoir to the pump and then through valves, flow meter(s) to the test channel and then back to the reservoir. Various test conditions were achieved by modifying flow rates, and by inserting different test models into the measurement section of the test channel.

Prior to velocity measurements, the PIV system was calibrated using the optimal background contrast and resolution settings. The field of view used was 27 mm per side so that the scale factor was typically 1.8. Peak-locking errors were minimized by ensuring that the particle image diameters were of 2.3 pixels (Raffel *et al.* 2007). To maintain a good signal to noise ratio, images acquisitions were done using laser pulses that were timed in such a way that the particle displacement in an interrogation area (IA) was less than a quarter of the side of the IA (Prasad, 2000). Using a typical interrogation window of 32 pixels by 32 pixels, and a sub-pixel accuracy of 0.1 (Scarano and Riethmuller, 1999), the dynamic range in the present tests is estimated to be 80. In choosing optimal time pulses, the ratio of the displacement field variation to the root mean square of the pixel size and particle image diameter was maintained at a value far less than 1 so that velocity gradient bias errors were kept minimal.

Vector correlations of images were obtained by post-processing camera-captured images using the fast-Fourier transform adaptive-correlation option of *Dantec Dynamic DynamicStudio* v.2.30 software. Accordingly, a Gaussian window function of width 0.1 pixels was used as an input filter, and a low-pass Gaussian output filter of width 1.8 pixels was chosen as a filter on the correlation plane prior to peak detection. Additionally, a dual-step correlation process of acceptance factor 0.05 was used to ensure that ample valid vectors were obtained. Two iterations were performed at the first step, and then one at the final step. The resultant spatial resolution was about 0.42 mm when the velocity data was processed using an interrogation window of size 32 pixels by 32 pixels. Using a 50% overlap between neighboring interrogation areas during the processing of data, additional vectors were provided

so that the distance between adjacent vectors was ~ 0.21 mm. Extensive velocity measurements were conducted at various sections of the streamwise/transverse (*x-y*) plane for various test conditions. The channel was moved along the streamwise/spanwise (*x-z*) in 2-mm intervals to measure the spanwise variations in velocity typically over 2-unit cells of the porous media.

Differential pressure measurements were concurrently made with the velocity measurements. Each of these pressure-measuring instruments was calibrated under standard conditions prior to measurements. Due to the high sensitivity of these instruments, they were connected and installed so that the potential for any clogging of the unit by seeding particles, and the effect of external vibrations was kept minimal. Further precautions were taken to ensure that bubbles in the tapping lines were bled off. To optimize the dynamic response of the instruments, the pressure lines were generally short, and of internal diameters of the order of 3 mm. The least count of the gauges were respectively 0.05 and 0.1 inches of water, for the 0 – 0.5 and 0 – 1 inches of water ranged 4000 Series *Capsuhelic* gauges. The least count of the DTD+ electronic transducer was 0.0002 inches of water. The differential pressure measurements were therefore computed from an average of the pressure differences recorded for each round of measurement. Most of the pressure measurements were done with the electronic transducer. This is because its precision was better, compared with the gauges.

2.6 Measurement Uncertainty

Several preliminary tests were conducted to determine the sample size of images required to attain statistical convergence of velocity data, determine the accuracy of the velocity data, optimize velocity measurement resolutions, verify the dimensionality of the horizontal porous media models, verify the accuracy of pressure measurements, and to estimate measurement uncertainties. With respect to the latter, a formal assessment was undertaken based on the methodology outlined by Coleman and Steele (1995) and Stern *et al.* (1999). The velocity and pressure uncertainties in measurements were determined using the bias and precision errors. In particular, the precision limit was obtained using a minimum of 11 experiments. Further details of this assessment are presented in Arthur (2012). The uncertainty in streamwise velocity u within the porous medium of $\phi = 6\%$ is estimated to be 1.5% of the local maximum velocity u_{max}. For model porous media of $\phi = 0.12, 0.22$, the uncertainties of u approximately 2.5%, and 4% respectively of u_{max}. For the transverse velocities v, total uncertainties are also estimated to be 1% of u_{max} and in porous media of $\phi = 6\%$; and 2% and 3% of u_{max} in model porous media of $\phi = 12\%, 22\%$ respectively. The total uncertainty in the differential pressure measurement is also estimated to be 3% of the average pressure drop. All error estimates are at 95% confidence level.

2.7 Test Conditions

The test conditions are summarized in Table 1. The geometrical descriptions of the models are also summarized. The Reynolds number $Re_d = (U_d d) / \nu$ was used in each case. Here, the seepage velocity U_d was obtained by averaging the velocities within the core of the porous media model. It is to be noted that for these experiments, the goal was to obtain measurements to cover the range of Re_d where inertia is non-existent, as well as just apparent (*i.e.* $0.1 < Re_d < 12.7$. However, this was not always possible because pressure values for $Re_d > 1$ exceeded the range that could be measured by the instruments that were used in this work.

Table 1 Summary of test conditions.

Model	Solid Volume Fraction ϕ	Range of U_d (mm/s)	Range of Re_d
Horizontal	6%	2.2 to 79.7	0.4 to 12.7
Horizontal	12%	2.6 to 25.0	0.4 to 4.0
Horizontal	22%	2.2 to 28.1	0.3 to 4.5
Mesh	6%	2.3 to 37.5	0.8 to 6.0
Mesh	12%	1.5 to 17.7	0.2 to 2.8
Mesh	22%	0.3 to 4.1	0.1 to 0.7

3. RESULTS AND DISCUSSION

In this section, results of particle image velocimetry and differential pressure measurements are presented with brief comments. It should be noted that particle image velocimetery provides a whole flow field of two-dimensional velocity measurements. However, the flow phenomena under consideration were mainly that of spatially averaged distributions. For the Cartesian frame of reference used in this work, the components of the microscopic (pore-level) velocity in the streamwise (x) and transverse (y) directions are designated respectively by u and v. Similarly, superficial velocities in the x and y directions are signified respectively by U_d and V_d.

3.1 Velocity Distribution

The section begins by drawing attention to some important observations from the averaged velocity results. In Fig. 4, the normalized pressure drop gradients (*i.e.* friction factors $f_{Ud} = (-dP_f /dx)(d/(\rho_f U_d^2))$, $f_{Vd} = (-dP_f /dx)(d/(\rho_f V_d^2))$ are plotted against the averaged velocities normalized by the recorded maximum superficial streamwise velocity $U_{d,max}$. This is done for the streamwise components (Fig. 4a) and transverse components (Fig. 4b) of the superficial velocity (respectively U_d and V_d) in log-linear plots. These are important depictions of the flow because it shows the relative contributions of the streamwise and transverse components of the velocity in the flow, and the variation of the friction factor with respect to the varying solid

volume fraction and dimensionality of the porous media. Furthermore, the presentation of the transverse components in particular in such an experiment is virtually non-existent in the literature.
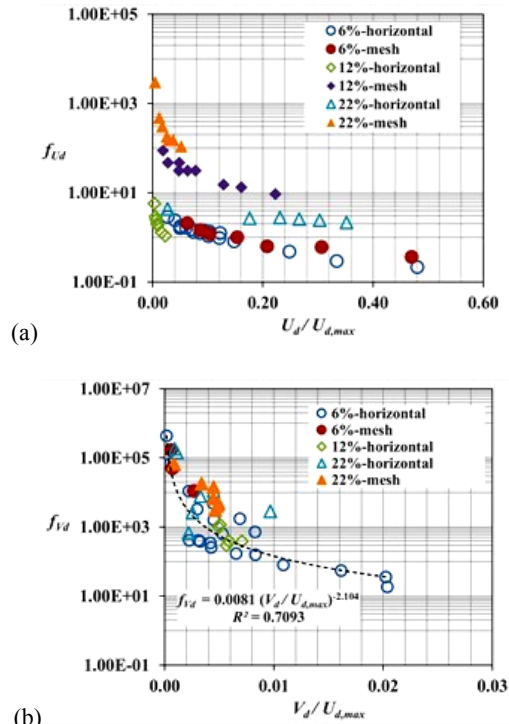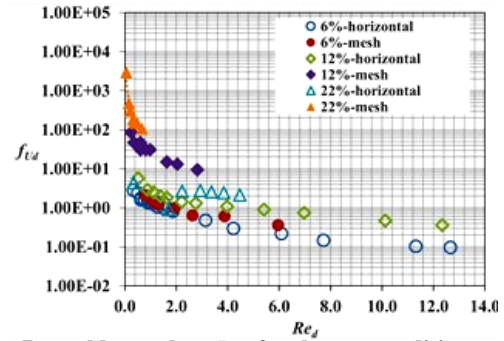

(a)

(b)

Fig. 4 (a) Friction factor $f_{Ud} = (-dP_f/dx)(d/\rho_f U_d^2)$ plotted against the averaged streamwise (U_d) velocities; and (b) friction factor $f_{Vd} = (-dP_f /dx)(d/\rho_f V_d^2)$ plotted against averaged transverse (V_d) averaged velocities for various test conditions.

The figures show that for each model, the normalized streamwise velocity measurements bear a quasi-power law relationship with the normalized pressure drop measurements. The results show that there is no discernible friction factor difference between the streamwise velocity models of two- or three-dimensionality for a solid volume fraction of 6%. However, the friction factor as the porous media solid volume fraction reaches 22%, the friction factor of the three-dimensional model porous media is much higher (about twenty times or more) than that of the two-dimensional porous media. These findings hint that as porous media tend to be more compact ($\phi > 12\%$), the effects of complexity play an important role in the global flow, magnifying the effects of the pressure drag and inertia. Indeed, the impact of inertia, through the streamwise velocities, is proven in Fig. 4(b). Those plots reveal that the differences in the flow phenomena for the various media are actually the result of the permeating influence of the streamwise velocity. When the streamwise velocities are discounted, the transverse components of the velocities, being much smaller than the streamwise velocities (by at least an order of magnitude), have a relatively little distinguishing effect on the flow

phenomena. They, therefore, yield high friction factor values that fall on the same power law, irrespective of the porous media.

3.2 The Force Interplay at the Onset of Forchheimer Regime

To investigate the forces at play at the onset of inertia, the streamwise flow data was studied further for both two- and three-dimensional porous media. This was done using the friction factor f_{Ud} (= $(-dP_f/dx)(d/(\rho_f U_d^2))$) and the characteristic Reynolds number Re_d (= $U_d\,d/\nu$). The log-linear plot of f_{Ud} against the characteristic particle Reynolds number Re_d in Fig. 5 shows that f_{Ud} reduces with increasing Re_d. Additionally, for a given Re_d, f_{Ud} increases with increasing solid volume fraction ϕ of the porous medium, and f_{Ud} of the mesh models is significantly higher than that of horizontal media. The f_{Ud} values of mesh models of $\phi = 12\%$ and 22%, in particular, are about ten times the value of the corresponding horizontal porous media. Again, in consonance with earlier observations, these results indicate that the friction factor increases as the porous medium becomes more compact and complex in arrangement. However, the question that remains is this – how do the forces at play really interact at this regime of inertia If f_{Ud} is interpreted as the ratio of the pressure drag to the inertial forces along the stream, and Re_d the ratio of inertial and viscous forces, then at the very least, a study of the relative proportions of pressure (normal) drag, inertial and viscous forces as Re_d increases will be helpful in providing a better picture regarding the evolution of inertia in the presence of complex porous media parameters. To study such relative contributions of forces, the pressure (normal or form) drag, viscous, and inertial forces were extracted from the measurement data and assessed individually. In Figs. 6 – 8, the distributions of the forces computed per unit area (stresses), are shown in dimensional (N/m²) and dimensionless (fractional) units. It is important to note the relevance of these three notable stresses. Two of these stresses – the normal and viscous stresses – are frictional (drag per unit area). The normal drag per unit area (approximated by the product of the characteristic diametrical length and the pressure gradient: $d(dP_f/dx))$) is the normal frictional stress induced by the pressure difference upon the flow. This is a direct result of the geometrical effects of the porous media. The viscous stresses (estimated by the product of the dynamic viscosity and the ratio of the superficial velocity and the characteristic diametrical length: $\mu_f U_d/d$), are the flow's characteristic tangential frictional stresses, responsible for smoothening out the microscopic heterogeneous velocity scales at neighboring points of the flow. The inertial stresses on the other hand, (estimated as $\rho_f U_d^2$) are the stresses that bring about the transfer of energy from large-scale components to small-scale components, thereby ensuring a characteristic heterogeneity in the flow. It is emphasized here that the values of the stresses shown in Figs. 6 – 8 are only estimates – they are only measures of the actual stresses. However, they provide a useful assessment of the relative proportions involved in the flow.

Reynolds number, Re_d for the test conditions.
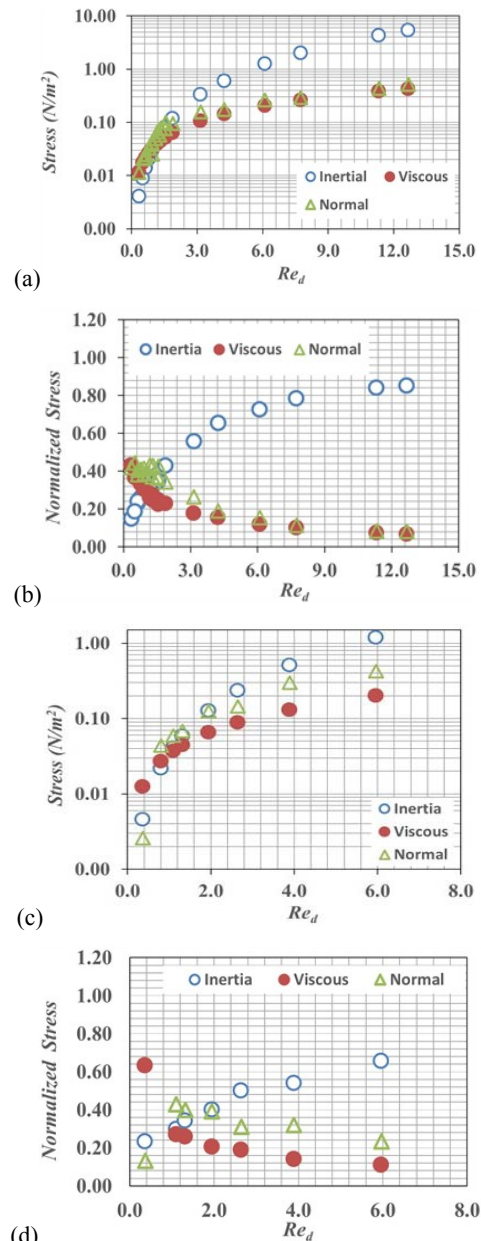

(a)

(b)

(c)

(d)

Fig. 6. The relative stress and normalized stress (*i.e.* stress divided by the sum of the inertial, viscous and normal stresses) distributions as Reynolds number Re_d increases for (a, b): horizontal porous media, (c, d): mesh porous media at $\phi = 6\%$.
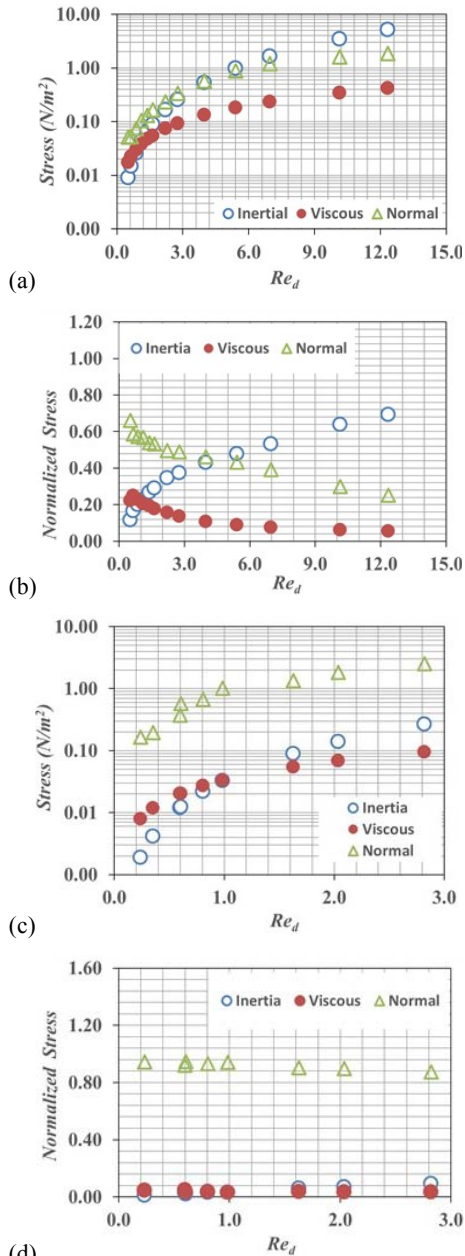
(a)

(b)

(c)

(d)

Fig. 7. The relative stress and normalized stress (*i.e.* stress divided by the sum of the inertial, viscous and normal stresses) distributions as Reynolds number Re_d increases for (a, b): horizontal porous media, (c, d): mesh porous media at ϕ = 12%.

Starting with the plots in Fig. 6, it is noted that for both porous media, the inertial stresses are the most dominant stresses at the Reynold number that inertia is expected to set in. However, each media shows a distinctive phenomenon. For the horizontal porous medium of φ = 6%, the friction and inertial stresses begin with similar values. However, by Re_d ~ 1 – 3, the inertial component shoots up considerably to ~60% of the sum of the inertial and frictional stresses, while the frictional stresses remain low and of similar values thereafter. The inertial stress increases exponentially from Re_d ~ 1 – 3 until peaking at Re_d ~ 12. In the case of the

mesh porous media, the normal form drag is significantly larger than (nearly twice) the viscous stresses as Re_d increases beyond 2. Thus, the normal drag grows significantly larger compared with the horizontal porous media (up to 150% more) as Re_d increases beyond 2. Comparatively, it would seem then that due to the impact of the form drag, the inertial forces are less subdued in the mesh porous medium, than the horizontal porous medium.
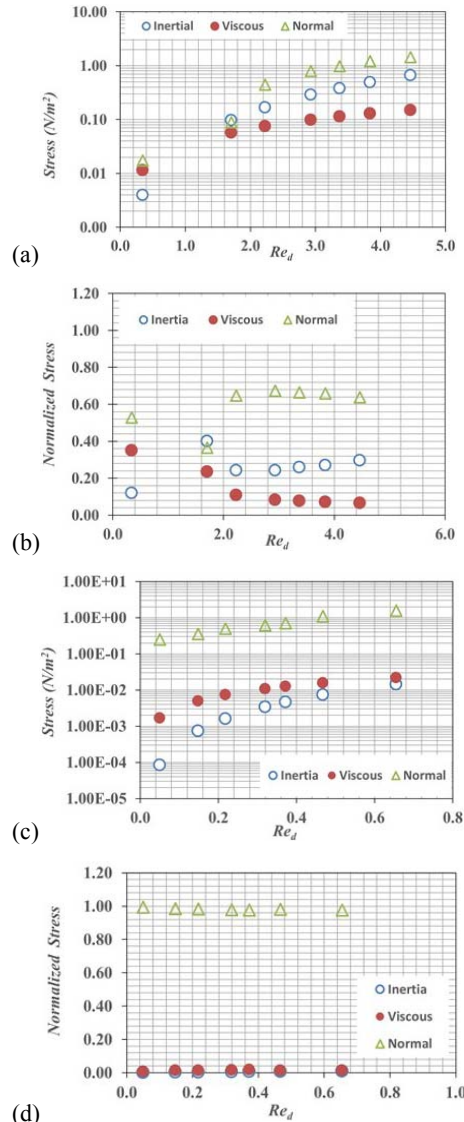

(a)

(b)

(c)

(d)

Fig. 8. The relative stress and normalized stress (*i.e.* stress divided by the sum of the inertial, viscous and normal stresses) distributions as Reynolds number Re_d increases for (a, b): horizontal porous media, (c, d): mesh porous media at ϕ = 22%.

In Fig. 7, the distinction between horizontal and porous media are much clearer than in Fig. 6. While the inertial stresses are the most dominant at the onset of inertial for horizontal porous media, for the mesh porous media, the normal frictional stresses are the most dominant throughout the flow. In Fig. 8, another picture is painted with respect to the differences between horizontal and mesh porous

media. For both media in Fig. 8, the most dominant stresses are that due to the normal drag, even though the mesh media seem to have 30% more compared with the horizontal media. The conclusion then is that as φ increases and the porous medium becomes more complex, the form drag expectedly becomes more prominent. However, a more important indication of these plots is the fact that as the form drag dominates the flow, it impedes the growth of inertia. This consequently leads to a wider transitional interval between the Darcy regime and the Forchheimer regime.

3.3 The Constitutive Equation at the Onset of Inertia

To explore the empirical equation that best applies to the flow for the conditions tested, the non-dimensionalized data (friction factor versus Reynolds number) were fitted to the best equation. Figure 9 shows the empirical fit for all test cases (except for mesh porous medium at 22% where that range of Reynolds number does not extend into the inertial regime range), together with the respective coefficient of determination, R^2. It is clear from the figure that the $f_{Ud} - Re_d$ relationship is that of a power law. To show which of the form of constitutive equation represented in the best line fit, non-dimensionalized forms of Eqs. (3) to (6), are derived as follows:

$$f_{Ud} = \frac{ad^2}{\mu Re_d} + \frac{db}{\rho} \tag{8}$$

$$f_{Ud} = \frac{ad^2}{Re_d\mu} + \left(\frac{dbU_d^{g-2}}{\rho}\right) \tag{9}$$

$$f_{Ud} = \frac{ad^2}{Re_d\mu} + \frac{db}{\rho} + \left(\frac{c}{\rho^2}Re_d\right) \tag{10}$$

$$f_{Ud} = \left(\frac{\mu\varepsilon U_d^{h-3}}{\rho^2}\right)Re_d = \alpha Re_d^{\beta} \tag{11}$$

where α and β are empirical values. Equation (11) indicates that the best-matched equation is that of Izbash (1931).
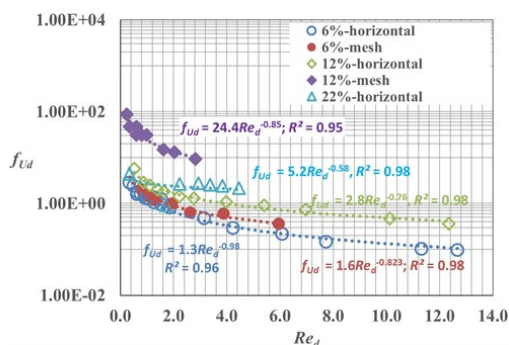

Fig. 9. The friction factor, f_{Ud} against the Reynolds number, Re_d for the test conditions except for 22% - mesh. The plots are presented with best line fits.

Writing Eq. (10) in terms of the Eq. (6) shows that the exponential parameter h is not a fixed number. It ranges between 1.10 and 1.42 for cases of flow extending into the onset of inertia. The results are summarized in Table 2. The data fall within the range of equivalent values published in several papers that put it between 1 and 2 (e.g. Basak, 1976, Bordier and Zimmer, 2000, Rong et al. 2016). Nothing conclusive can be said about the difference between two- and three-dimensional porous media results in the data presented in Table 2. However, for the two-dimensional horizontal porous medium, it is worth noting that the parameter h tends to reduce with increasing solid volume fraction φ. This implies the deviation from the Darcy law at the onset of inertia is less obvious at low φ, and that at lower than 6%, the Darcy law may be sufficient to describe the flow at the Forchheimer regime. The results also indicate that, a single equation may be feasible for flow in both Darcian and Forchheimer regime, especially for porous media of very low solid volume fraction. This is something to be explored in future work.

Table 2 Data results of parameter h

Porous Medium	h	Re_d
6%-horizontal	1.10	0.4 to 12.7
12%-horizontal	1.24	0.4 to 4.0
22%-horizontal	1.42	0.3 to 4.5
6%-mesh	1.18	0.8 to 6.0
12%-mesh	1.15	0.2 to 2.8

4. CONCLUSIONS

In this work, particle image velocimetry and pressure measurements of flow through model porous media have been used to investigate the flow at the onset of inertia.

Using the velocity and pressure measurements and fluid density and viscosity, the following conclusions are evident:

a) The streamwise flow dictates the flow phenomenon. When the streamwise velocities are discounted, the transverse components of the velocities, being much smaller than the streamwise velocities (by at least an order of magnitude), show little differences in flow phenomenon in different media. They thus result in high friction factor values that fall on the same power law, irrespective of the porous media.

b) The more compact ($\phi > 12\%$), and more complex (three-dimensional compared with two-dimensional) the porous media, the more magnified are the effects of the pressure drag.

c) An evaluation of stresses shows that inertia increases exponentially from particle Reynolds number between $\sim 1 - 3$.

d) There is an indication that as the form drag dominates the flow, it impedes the growth of inertia. This consequently leads to a wider transitional interval between the Darcy regime

and the Forchheimer regime.

e) The equation given by Izbash (1931) best reflects the porous media flow at the onset of inertia.

f) For the two-dimensional porous medium, as the solid volume fraction becomes less and less, the Darcy law may be sufficient to describe the flow at the Forchheimer regime.

To further solidify the above-mentioned conclusions for a wider range of Reynolds numbers and porous media types, further experimental work and numerical analyses are required. However, this work provides reasonable and further concrete basis to use the Izbash (1931) equation at the onset of inertia for all sorts of porous media, as applicable to modeling of fluid flows pertaining to near well bores, fractures and tight screens of cryogenic propellant tanks.

ACKNOWLEDGEMENTS

REFERENCES

Arthur, J. K. (2012). *Flow Through and Over Porous Media with or without Inertial Effects.* Ph.D. thesis, University of Manitoba, Winnipeg, Manitoba, Canada.

Barree, R. D. and M. Y. Conway (2004). Beyond beta factors: A complete model for Darcy, Forchheimer and Trans-Forchheimer flow in porous media. In *Proceedings of the SPE Annual Technical Conference and Exhibition*, Houston, Texas, USA.

Barree, R. D. and M. W. Conway (2005). Reply to discussion of 'Beyond beta factors: a complete model for Darcy, Forchheimer, and Trans-Forchheimer flow in porous media'. *Journal of Petroleum Technology* 57(8), 73–74.

Basak, P. (1977). Non-Darcy flow and its implications to seepage problems. *Journal of the Irrigation and Drainage Division*, 103 (IR4), 459–473.

Bordier, C. and D. Zimmer (2000). Drainage equations and non-Darcian modeling in coarse porous media or geosynthetic materials. *Journal of Hydrology* 228, 174–187.

Chauveteau, G. (1965). *Essai sur la loi de Darcy.* Ph.D. thesis, University of Toulouse, Toulouse, France.

Coleman, W. H. and W. G. Steele (1995). Engineering application of experimental uncertainty analysis. American Institute of Aeronautics and Astronautics 33, 1888–1896.

Darcy, H. P. G. (1856). *Les Fontaines Publiques de la Ville de Dijon.* Paris: Victor Dalmont, France.

Dybbs, A. and R. V. Edwards (1984). A new look at porous media fluid mechanics—Darcy to turbulent, In: *Fundamentals of Transport Phenomena in Porous Media Flow.* Martinus Nishoff, Dordrecht, Holland.

Escande, L (1953). Experiments concerning the filtration of water through rockmass. In *Proceedings of Minnesota International Hydraulic Convention,* Minnesota, United States of America.

Firdaous, M., J. L. Guermond and P. Le Quéré (1997). Nonlinear corrections to Darcy's law at low Reynolds numbers. *Journal of Fluid Mechanics* 343, 331 – 350.

Forchheimer, P. (1930). *Hydraulik.* 3rd edn. Teubner, Leipzig, Germany.

Forchheimer, P. (1901). Wasserberwegung durch boden. *Z. Vereines deutscher Ing.* 45 (50), 1782–1788.

Hayes, R. E., A. Afacan and B. Boulanger (1995). An equation of motion for an in-compressible Newtonian fluid in a packed bed. *Transport in Porous Media* 18, 185 – 198.

Hazen, A. (1895). *The Filtration of Public Water-Supplies.* Wiley, New York, United States of America.

Hlushkou, D. and U. Tallarek (2006). Transition from creeping via viscous-inertial to turbulent flow in fixed beds. *Journal of Chromatography A*, 1126, 70 – 85.

Izbash, S. V. (1931). *O fitracii v Krupnozernstom Materiale, Izr. Nauchno-isoled, Qust. Gidrotechniki.* (NIIG), Leningrad.

Ma, H. and D. W. Ruth (1993). The microscopic analysis of high Forchheimer number flow in porous media. Transport in Porous Media 13, 139 – 160.

Marušic–Paloka, E. and A. Mikelic (2000). The derivation of a non-linear filtration law including the inertia effects via homogenization. *Nonlinear Analysis Theory Methods and Application* 42, 97 – 137.

Mei, C. C. and J. L. Auriault (1991). The effect of weak inertia on flow through a porous medium. *Journal of Fluid Mechanics* 222, 647 – 663.

Minsky, E. M. (1951). On the turbulent flow through porous media. *Dokl Acad Nauk SSSR* 58(3), 409– 412.

Moutsopoulos, K. N. and V. A. Tsihrintzis (2005). Approximate analytical solutions of the Forchheimer equation. *Journal of Hydrology* 309, 93 – 103.

Panfilov, M., C. Oltean, I. Panfilova and M. Bues (2003). Singular nature of nonlinear macroscale effects in high-rate flow through

porous media. *Comtes Rendus Mecanique* 331, 41 – 48.

Prasad, A. K. (2000). Particle image velocimetry. *Current Science* 79(1), 51-60.

Raffel, M., C., Willert, S. Wereley and J. Kompenhans (2007). *Particle Image Velocimetry. A Practical Guide*. 2nd Edn. Springer Verlag, Berlin, Heidelberg, New York, United States of America.

Rong, G., J. Yang, L. Cheng and C. Zhou (2016). Laboratory investigation of nonlinear flow characteristics in rough fractures during shear. *Journal of Hydrology*, 541, 1385–1394.

Ruth, D. W. and H. Ma (1992). On the derivation of the Forchheimer equation by means of the averaging theorem. *Transport in Porous Media* 7, 255 – 264.

Scarano F. and M. L. Riethmuller (1999). Iterative multigrid approach in PIV image processing with discrete window offset. *Experiments in Fluids*, 26(6), 513 - 523.

Scheidegger, A. E. (1960). *The Physics of Flow through Porous Media*. University of Toronto Press, Toronto, Canada.

Sedghi-Asl, M., M. Salahi and M. Parvizi (2015). Nonlinear flow through a packed-column experiment. *Journal of Hydrologic Engineering* 20(9), 04015003-1 - 04015003-9.

Skjetne, E., A. Hansen and J. S. Gudmundsson (1999). High-velocity flow in a rough fracture. *Journal of Fluid Mechanics* 383, 1 – 28.

Slepicka, F. (1961). Hydraulic function of cylindrical well in an artesian aquifer with regard to new research on flow through porous media. In *Proceedings of IAHR, 9th Congress*, Dubrovnik, Croatia.

Stern, F., M. Muste, M. Beninati and W. E. Eichinger (1999). Summary of experimental uncertainty assessment methodology with example. *IIHR Technical Report*, 406.

Whitaker, S. (1996). The Forchheimer equation: a theoretical development. *Transport in Porous Media* 25, 27 – 62.

White, A. M. (1935). *Transactions of the American Institute of Chemical Engineers*, 31, 390. In: J. Bear, *Dynamics of Fluid Flow through Porous Media*. Dover, New York, United States of America.

Wilkinson, J. K. (1956). The flow of water through rockfill and application to the design of dams. In *Proceedings of the 2nd Australia-New Zealand Conference on Soil Mechanics and Foundation Engineering*, Melbourne, Australia.

Wooding, R. A. (1957). Steady-state free thermal convection of liquid in a saturated permeable medium. *Journal of Fluid Mechanics* 2, 273 – 285.